Research Article

Timothy Kitungu Nzomo*, Stephen Ezizanami Adewole, Kennedy Otieno Awuor and Daniel Okang'a Oyoo

Performance of a horizontal well in a bounded anisotropic reservoir: Part II: Performance analysis of well length and reservoir geometry

https://doi.org/10.1515/eng-2022-0477
received May 22, 2021; accepted June 12, 2023

Abstract: Evaluation of the performance of horizontal wells is an important aspect in the enhancement of their productivity. This study provides mathematical computations, and analysis for theoretical well and reservoir considerations. The study investigates how well design and reservoirs geometry affect the overall performance of a horizontal well in a completely bounded reservoir throughout its productive life. A horizontal well in a rectangular reservoir with completely sealed boundaries is considered and the effect of dimensionless well length L_D, dimensionless reservoir length x_{eD}, and dimensionless reservoir width y_{eD} on the pressure response over a given period of production using dimensionless time t_D is studied. The mathematical model used was derived using source and Green's functions presented in part **I** of this study. Appropriate well and reservoir parameters are considered and the respective dimensionless parameters are computed which are then used in computing dimensionless pressure P_D and its dimensionless pressure derivative P_D'. From the computations, the results obtained are analysed in diagnostic log–log plots with a discussion of the flow periods. The results obtained indicate that an increase in dimensionless well length decreases pressure response during the infinite-acting flow at early times and during transition flows at middle time but increases the pressure response during the pseudosteady state flow at late times. The dimensionless reservoir width and length are observed not to influence dimensionless pressure response during the infinite-acting flow at early times and during the transition flows at middle time, only affecting the prevalence time of the flow periods. However it is observed that during the pseudosteady state flow at late times, dimensionless pressure response reduces with increased dimensionless reservoir length and width.

Keywords: horizontal well length, reservoir geometry, pressure distribution, pseudosteady state flow

1 Introduction

The performance of any well will depend on its initial design and any improvements that can be made to enhance its productivity. Analysis of horizontal wells has continued to pose challenges due to the complexity when it comes to analysing the flow periods with several boundaries involved. This is due to the occurrence of transient and pseudosteady flows as different boundaries are affected. Previous studies [1–20] as discussed in part I [21] of this study have made major strides in studying pressure response in horizontal wells. However, the considerations of infinite-acting, separate sealed boundaries, and isotropy in calculations have continued posing challenges to the accuracy of results obtained. The consideration of completely sealed boundaries and a study of pressure response from inception to date have not been fully considered. In this study, by including individual directional permeabilities in computations, the effect of well length and reservoir geometry on the performance of a horizontal well from inception to date is investigated.

2 Reservoir description

The well and reservoir geometry is as described in Figure 1 and the well is considered to be centrally placed in the

* **Corresponding author: Timothy Kitungu Nzomo**, Mathematics Department, Kenyatta University, Box 43844-00100, Nairobi, Kenya, e-mail: nzomotimothy@gmail.com
Stephen Ezizanami Adewole: Gas and Petroleum Engineering Department, Kenyatta University, Box 43844-00100, Nairobi, Kenya
Kennedy Otieno Awuor: Mathematics Department, Kenyatta University, Box 43844-00100, Nairobi, Kenya
Daniel Okang'a Oyoo: Gas and Petroleum Engineering Department, Kenyatta University, Box 43844-00100, Nairobi, Kenya

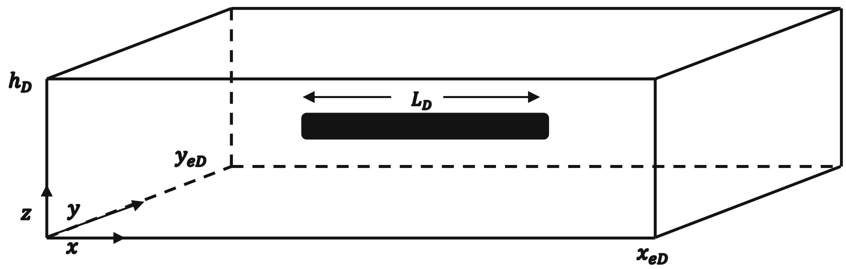

Figure 1: Horizontal well in a rectangular drainage volume.

reservoir. The drainage volume considered is completely sealed in all axes.

3 Mathematical description

It is assumed that the vertical boundary will be felt first since the formation thickness is expected to be far much smaller compared to the width and length of a given reservoir. The mathematical model used considers two possible cases obtained from previous studies [22] and [23]. First, a case where the horizontal boundary parallel to the well (y-boundary) is felt first. In this case, the dimensionless pressure derived in part I [21] of this study is given by equation (1) and its equivalent dimensionless derivative is given by equation (2).

$$
\begin{aligned}
P_{\mathrm{D}} = {} & -\frac{\beta h_{\mathrm{D}} k}{4\sqrt{k_y k_z}}\mathrm{Ei}\left(-\frac{r_{\mathrm{wD}}{}^2}{4t_{\mathrm{De}}}\right) + \frac{\sqrt{\pi}}{2}\sqrt{\frac{k}{k_y}}\int_{t_{\mathrm{De}}}^{t_{\mathrm{D1}}}\left\{\mathrm{erf}\left[\left(\frac{\sqrt{k/k_x} + (x_{\mathrm{D}} - x_{\mathrm{wD}})}{2\sqrt{\tau_{\mathrm{D}}}}\right)\right] + \mathrm{erf}\left[\left(\frac{\sqrt{k/k_x} - (x_{\mathrm{D}} - x_{\mathrm{wD}})}{2\sqrt{\tau_{\mathrm{D}}}}\right)\right]\right]\left[\exp\left(-\frac{(y_D - y_{\mathrm{wD}})^2}{4\tau_{\mathrm{D}}}\right)\right]\left[1\right.\\
& \left. + 2\sum_{l=1}^{\infty}\exp\left(-\frac{l^2\pi^2\tau_{\mathrm{D}}}{h_{\mathrm{D}}{}^2}\right)\cos\frac{l\pi z_{\mathrm{wD}}}{h_{\mathrm{D}}}\cos\frac{l\pi z_{\mathrm{D}}}{h_{\mathrm{D}}}\right]\Bigg\}\frac{\mathrm{d}\tau_{\mathrm{D}}}{\sqrt{\tau_D}}\\
& + \frac{\pi}{y_{\mathrm{eD}}}\int_{t_{\mathrm{D1}}}^{t_{\mathrm{D2}}}\left\{\left[\mathrm{erf}\left(\frac{\sqrt{k/k_x} + (x_{\mathrm{D}} - x_{\mathrm{wD}})}{2\sqrt{\tau_{\mathrm{D}}}}\right) + \mathrm{erf}\left(\frac{\sqrt{k/k_x} + (x_{\mathrm{D}} - x_{\mathrm{wD}})}{2\sqrt{\tau_{\mathrm{D}}}}\right)\right]\cdot\left[1 + 2\sum_{m=1}^{\infty}\exp\left(-\frac{m^2\pi^2\tau_{\mathrm{D}}}{y_{\mathrm{eD}}{}^2}\right)\cos\frac{m\pi y_{\mathrm{wD}}}{y_{\mathrm{eD}}}\cos\frac{m\pi y_{\mathrm{D}}}{y_{\mathrm{eD}}}\right]\cdot\left[1\right.\right.\\
& \left.\left. + 2\sum_{l=1}^{\infty}\exp\left(-\frac{l^2\pi^2\tau_{\mathrm{D}}}{h_{\mathrm{D}}{}^2}\right)\cos\frac{l\pi z_{\mathrm{wD}}}{h_{\mathrm{D}}}\cos\frac{l\pi z_{\mathrm{D}}}{h_{\mathrm{D}}}\right]\right\}\mathrm{d}\tau_{\mathrm{D}}\\
& + \frac{2\pi}{x_{\mathrm{eD}}y_{\mathrm{eD}}}\int_{t_{\mathrm{D2}}}^{t_{\mathrm{D}}}\left[\left[1 + \frac{2x_{\mathrm{eD}}}{\pi}\sum_{n=1}^{\infty}\frac{1}{n}\exp\left(-\frac{n^2\pi^2\tau_{\mathrm{D}}}{x_{\mathrm{eD}}{}^2}\right)\sin\frac{n\pi}{x_{\mathrm{eD}}}\cos\frac{n\pi x_{\mathrm{wD}}}{x_{\mathrm{eD}}}\cos\frac{n\pi x_{\mathrm{D}}}{x_{\mathrm{eD}}}\right]\cdot\left[1\right.\right.\\
& \left.\left. + 2\sum_{m=1}^{\infty}\exp\left(-\frac{m^2\pi^2\tau_{\mathrm{D}}}{y_{\mathrm{eD}}{}^2}\right)\cos\frac{m\pi y_{\mathrm{wD}}}{y_{\mathrm{eD}}}\cos\frac{m\pi y_{\mathrm{D}}}{y_{\mathrm{eD}}}\right]\cdot\left[1 + 2\sum_{l=1}^{\infty}\exp\left(-\frac{l^2\pi^2\tau_{\mathrm{D}}}{h_{\mathrm{D}}{}^2}\right)\cos\frac{l\pi z_{\mathrm{wD}}}{h_{\mathrm{D}}}\cos\frac{l\pi z_{\mathrm{D}}}{h_{\mathrm{D}}}\right]\right]\mathrm{d}\tau_{\mathrm{D}},
\end{aligned}
\tag{1}
$$

$$
\begin{aligned}
P'_{\mathrm{D}} = {} & \frac{\beta h_{\mathrm{D}} k}{4\sqrt{k_y k_z}}\exp\left(-\frac{r_{\mathrm{wD}}{}^2}{4t_{\mathrm{D}}}\right) + \frac{\sqrt{\pi}}{2}\sqrt{\frac{k}{k_y}}\left\{\mathrm{erf}\left[\left(\frac{\sqrt{k/k_x} + (x_{\mathrm{D}} - x_{\mathrm{wD}})}{2\sqrt{t_{\mathrm{D}}}}\right)\right] + \mathrm{erf}\left[\left(\frac{\sqrt{k/k_x} - (x_{\mathrm{D}} - x_{\mathrm{wD}})}{2\sqrt{t_{\mathrm{D}}}}\right)\right]\right]\left[\exp\left(-\frac{(y_D - y_{\mathrm{wD}})^2}{4t_{\mathrm{D}}}\right)\right]\left[1\right.\\
& \left. + 2\sum_{l=1}^{\infty}\exp\left(-\frac{l^2\pi^2 t_{\mathrm{D}}}{h_{\mathrm{D}}{}^2}\right)\cos\frac{l\pi z_{\mathrm{wD}}}{h_{\mathrm{D}}}\cos\frac{l\pi z_{\mathrm{D}}}{h_{\mathrm{D}}}\right]\Bigg\}\sqrt{t_{\mathrm{D}}} + \frac{\pi}{y_{\mathrm{eD}}}\left\{\left[\mathrm{erf}\left(\frac{\sqrt{k/k_x} + (x_{\mathrm{D}} - x_{\mathrm{wD}})}{2\sqrt{t_{\mathrm{D}}}}\right) + \mathrm{erf}\left(\frac{\sqrt{k/k_x} + (x_{\mathrm{D}} - x_{\mathrm{wD}})}{2\sqrt{t_{\mathrm{D}}}}\right)\right]\cdot\left[1\right.\right.\\
& \left.\left. + 2\sum_{m=1}^{\infty}\exp\left(-\frac{m^2\pi^2 t_{\mathrm{D}}}{y_{\mathrm{eD}}{}^2}\right)\cos\frac{m\pi y_{\mathrm{wD}}}{y_{\mathrm{eD}}}\cos\frac{m\pi y_{\mathrm{D}}}{y_{\mathrm{eD}}}\right]\cdot\left[1 + 2\sum_{l=1}^{\infty}\exp\left(-\frac{l^2\pi^2 t_{\mathrm{D}}}{h_{\mathrm{D}}{}^2}\right)\cos\frac{l\pi z_{\mathrm{wD}}}{h_{\mathrm{D}}}\cos\frac{l\pi z_{\mathrm{D}}}{h_{\mathrm{D}}}\right]\right\}t_{\mathrm{D}}\\
& + \frac{2\pi}{x_{\mathrm{eD}}y_{\mathrm{eD}}}\left\{\left[1 + \frac{2x_{\mathrm{eD}}}{\pi}\sum_{n=1}^{\infty}\frac{1}{n}\exp\left(-\frac{n^2\pi^2 t_{\mathrm{D}}}{x_{\mathrm{eD}}{}^2}\right)\sin\frac{n\pi}{x_{\mathrm{eD}}}\cos\frac{n\pi x_{\mathrm{wD}}}{x_{\mathrm{eD}}}\cos\frac{n\pi x_{\mathrm{D}}}{x_{\mathrm{eD}}}\right]\cdot\left[1\right.\right.\\
& \left.\left. + 2\sum_{m=1}^{\infty}\exp\left(-\frac{m^2\pi^2 t_{\mathrm{D}}}{y_{\mathrm{eD}}{}^2}\right)\cos\frac{m\pi y_{\mathrm{wD}}}{y_{\mathrm{eD}}}\cos\frac{m\pi y_{\mathrm{D}}}{y_{\mathrm{eD}}}\right]\cdot\left[1 + 2\sum_{l=1}^{\infty}\exp\left(-\frac{l^2\pi^2 t_{\mathrm{D}}}{h_{\mathrm{D}}{}^2}\right)\cos\frac{l\pi z_{\mathrm{wD}}}{h_{\mathrm{D}}}\cos\frac{l\pi z_{\mathrm{D}}}{h_{\mathrm{D}}}\right]\right\}t_{\mathrm{D}}.
\end{aligned}
\tag{2}
$$

Second, a case where the horizontal boundary perpendicular to the well (x-boundary) is felt first, the dimensionless pressure as derived from part I of this study is given by equation (3) and its equivalent dimensionless pressure derivative is given by equation (4).

$$\begin{aligned}P_D = &-\frac{\beta h_D k}{4\sqrt{k_y k_z}}\mathrm{Ei}\left(-\frac{r_{wD}^2}{4t_{De}}\right) + \frac{\sqrt{\pi}}{2}\sqrt{\frac{k}{k_y}}\int_{t_{De}}^{t_{D1}}\left\{\mathrm{erf}\left[\left(\frac{\sqrt{k/k_x} + (x_D - x_{wD})}{2\sqrt{\tau_D}}\right)\right] + \mathrm{erf}\left[\left(\frac{\sqrt{k/k_x} - (x_D - x_{wD})}{2\sqrt{\tau_D}}\right)\right]\left[\exp\left(-\frac{(y_D - y_{wD})^2}{4\tau_D}\right)\right]\right[1\\
&+ 2\sum_{l=1}^{\infty}\exp\left(-\frac{l^2\pi^2\tau_D}{h_D^2}\right)\cos\frac{l\pi z_{wD}}{h_D}\cos\frac{l\pi z_D}{h_D}\bigg]\bigg\}\frac{d\tau_D}{\sqrt{\tau_D}}\\
&+ \frac{\sqrt{\pi}}{x_{eD}}\sqrt{\frac{k}{k_y}}\int_{t_{D1}}^{t_{D2}}\left\{\left[1 + \frac{2x_{eD}}{\pi}\sum_{n=1}^{\infty}\frac{1}{n}\exp\left(-\frac{n^2\pi^2\tau_D}{x_{eD}^2}\right)\sin\frac{n\pi}{x_{eD}}\cos\frac{n\pi x_{wD}}{x_{eD}}\cos\frac{n\pi x_D}{x_{eD}}\right]\left[\exp\left(-\frac{(y_D - y_{wD})^2}{4\tau_D}\right)\right]\right[1\\
&+ 2\sum_{l=1}^{\infty}\exp\left(-\frac{l^2\pi^2\tau_D}{h_D^2}\right)\cos\frac{l\pi z_{wD}}{h_D}\cos\frac{l\pi z_D}{h_D}\bigg]\bigg\}\frac{d\tau_D}{\sqrt{\tau_D}}\\
&+ \frac{2\pi}{x_{eD}y_{eD}}\int_{t_{D2}}^{t_D}\left\{\left[1 + \frac{2x_{eD}}{\pi}\sum_{n=1}^{\infty}\frac{1}{n}\exp\left(-\frac{n^2\pi^2\tau_D}{x_{eD}^2}\right)\sin\frac{n\pi}{x_{eD}}\cos\frac{n\pi x_{wD}}{x_{eD}}\cos\frac{n\pi x_D}{x_{eD}}\right]\cdot\right[1\\
&+ 2\sum_{m=1}^{\infty}\exp\left(-\frac{m^2\pi^2\tau_D}{y_{eD}^2}\right)\cos\frac{m\pi y_{wD}}{y_{eD}}\cos\frac{m\pi y_D}{y_{eD}}\bigg]\cdot\left[1 + 2\sum_{l=1}^{\infty}\exp\left(-\frac{l^2\pi^2\tau_D}{h_D^2}\right)\cos\frac{l\pi z_{wD}}{h_D}\cos\frac{l\pi z_D}{h_D}\right]\bigg\}d\tau_D,\end{aligned} \tag{3}$$

$$\begin{aligned}P_D' = &\frac{\beta h_D k}{4\sqrt{k_y k_z}}\exp\left(-\frac{r_{wD}^2}{4t_D}\right) + \frac{\sqrt{\pi}}{2}\sqrt{\frac{k}{k_y}}\left\{\mathrm{erf}\left[\left(\frac{\sqrt{k/k_x} + (x_D - x_{wD})}{2\sqrt{t_D}}\right)\right] + \mathrm{erf}\left[\left(\frac{\sqrt{k/k_x} - (x_D - x_{wD})}{2\sqrt{t_D}}\right)\right]\left[\exp\left(-\frac{(y_D - y_{wD})^2}{4t_D}\right)\right]\right[1\\
&+ 2\sum_{l=1}^{\infty}\exp\left(-\frac{l^2\pi^2 t_D}{h_D^2}\right)\cos\frac{l\pi z_{wD}}{h_D}\cos\frac{l\pi z_D}{h_D}\bigg]\bigg\}\sqrt{t_D}\\
&+ \frac{\sqrt{\pi}}{x_{eD}}\sqrt{\frac{k}{k_y}}\left\{\left[1 + \frac{2x_{eD}}{\pi}\sum_{n=1}^{\infty}\frac{1}{n}\exp\left(-\frac{n^2\pi^2 t_D}{x_{eD}^2}\right)\sin\frac{n\pi}{x_{eD}}\cos\frac{n\pi x_{wD}}{x_{eD}}\cos\frac{n\pi x_D}{x_{eD}}\right]\left[\exp\left(-\frac{(y_D - y_{wD})^2}{4t_D}\right)\right]\right.\\
&\times\left[1 + 2\sum_{l=1}^{\infty}\exp\left(-\frac{l^2\pi^2 t_D}{h_D^2}\right)\cos\frac{l\pi z_{wD}}{h_D}\cos\frac{l\pi z_D}{h_D}\right]\bigg\}\sqrt{t_D}\\
&+ \frac{2\pi}{x_{eD}y_{eD}}\left\{\left[1 + \frac{2x_{eD}}{\pi}\sum_{n=1}^{\infty}\frac{1}{n}\exp\left(-\frac{n^2\pi^2 t_D}{x_{eD}^2}\right)\sin\frac{n\pi}{x_{eD}}\cos\frac{n\pi x_{wD}}{x_{eD}}\cos\frac{n\pi x_D}{x_{eD}}\right]\cdot\right[1\\
&+ 2\sum_{m=1}^{\infty}\exp\left(-\frac{m^2\pi^2 t_D}{y_{eD}^2}\right)\cos\frac{m\pi y_{wD}}{y_{eD}}\cos\frac{m\pi y_D}{y_{eD}}\bigg]\cdot\left[1 + 2\sum_{l=1}^{\infty}\exp\left(-\frac{l^2\pi^2 t_D}{h_D^2}\right)\cos\frac{l\pi z_{wD}}{h_D}\cos\frac{l\pi z_D}{h_D}\right]\bigg\}t_D.\end{aligned} \tag{4}$$

4 Results and discussion

Theoretical well and reservoir parameters for a centrally located well in a single layer such that $m = n = l = 1$ are considered and their respective dimensionless equivalents are computed. A line source is considered such that $y_D = y_{wD}$ and $r_{wD} = z_D - z_{wD}$. A monitoring point at the centre of the well such that $x_D = x_{wD}$ approximates $\beta = 2$ during early time. Using Odeh and Babu Strategies discussed in part I [21] of this study, the approximate integration limits are identified. To compute dimensionless pressure and its dimensionless pressure derivative, all the considered and computed parameters are substituted into the models. The results are presented and analysed in diagnostic log–log plots.

4.1 Effect of dimensionless horizontal well length

To study how the dimensionless horizontal well length, L_D affects the flow periods and dimensionless pressure, dimensionless horizontal well length is varied keeping

Table 1: Dimensional and dimensionless parameters for different values of L_D

L (ft)	k_x = 200 md, k_y = 150 md, k_z = 10 md, h = 150 ft, x_e = 30,000 ft, y_e = 20,000 ft								
	L_D	x_{wD}	x_{eD}	r_{wD}	y_{wD}	y_{eD}	z_D	z_{wD}	h_D
500	0.9642	34.713	69.426	0.0031	26.722	53.444	0.7793	0.7762	1.5524
1,000	1.9285	17.356	34.713	0.0016	13.361	26.722	0.3897	0.3881	0.7762
1,500	2.8927	11.571	23.142	0.0010	8.9073	17.815	0.2598	0.2587	0.5175
2,000	3.8570	8.6782	17.356	0.0008	6.6805	13.361	0.1948	0.1941	0.3881
2,500	4.8212	6.9426	13.885	0.0006	5.3444	10.689	0.1559	0.1552	0.3105

the other parameters constant. Table 1 shows the theoretical dimensional values considered and the computed dimensionless variables.

Table 2 shows the dimensionless flow period times as computed using Odeh and Babu strategies. From Table 2, it is observed that the y-boundary is felt first. Using equation (1), dimensionless pressure is computed, and dimensional pressure derivative is computed using equation (2).

The dimensionless pressure and dimensionless pressure derivative values computed are shown in Table 3. Figure 2 shows the plot of P_D and P_D' against t_D on log–log axes where the solid lines represent P_D against t_D, while the dashed lines represent P_D' against t_D. From Figure 2, the infinite-acting flow is identified as the first flow period. This flow period starts shortly after the well is put into production. This flow period is evident with the flattening of the dimensionless pressure derivative plot at early times. This flow period is radial in the y–z plane and can be considered as the early radial flow period. It is noted that this flow period might end even before the vertical boundary is felt for the cases where the flow coming from the ends of the well starts influencing the pressure response. In such a case, a very short transition flow which is still radial continues until the flow reaches the vertical boundary. When the vertical boundary is felt, it is noted that as the dimensionless horizontal well length increases, an early linear flow period occurs in the y–z plane. This flow period is observed to prevail for a very short time and is evident when the dimensionless pressure derivative plot stops flattening and shows an upward trend. Where the early linear flow period does not occur, a transition flow occurs from the time the vertical boundary is felt until the time the flow starts coming from beyond the ends of the wellbore. This is evident for the first two cases of dimensionless horizontal well length considered. Where the early linear flow occurs as shown in the last three cases of the dimensionless horizontal well length considered, the period will end when the flow moves beyond the ends of the wellbore. At this point a transition flow occurs until the flow starts coming from beyond the ends of the wellbore. When the transition flow ends, a second radial flow is identified with the flattening of the graph of dimensionless pressure derivative. This flow period starts after the flow has started coming from beyond the ends of the wellbore and can be considered to be the late pseudoradial flow period with one boundary having been felt. This flow period will end when the y-boundary is felt which is followed by a transition flow.

The transition flow will prevail until the x-boundary is felt at a point where it can be considered that all boundaries have been felt and a pseudosteady state flow begins. On the plot, this is identified with the straight upward line at late time. This flow period will prevail to date. For the parameters considered, it is noted that as the dimensionless horizontal well length increases, the pressure response decreases during early time but increases during late time when a pseudosteady state behaviour is observed.

Table 2: Dimensionless flow period times for different values of L_D

L (ft)	Early radial		Early linear		Late pseudoradial			Late linear		
	t_{De}	t_{De}	$t_{D(start)}$	$t_{D(end)}$	$t_{D(start)}$	$t_{D(end)}$	$t_{D(end)}$	$t_{D(start)}$	$t_{D(start)}$	$t_{D(end)}$
500	0.2863	0.0442	0.2863	0.0566	0.5231	625.67	311.05	1476.5	0.2863	311.05
1,000	0.0716	0.0442	0.0716	0.0566	0.5231	153.80	77.761	356.71	0.0716	77.761
1,500	0.0318	0.0442	0.0318	0.0566	0.5231	67.202	34.561	153.12	0.0318	34.561
2,000	0.0179	0.0442	0.0179	0.0566	0.5231	37.158	19.440	83.134	0.0179	19.440
2,500	0.0115	0.0442	0.0115	0.0566	0.5231	23.373	12.442	51.323	0.0115	12.442

Table 3: Dimensionless pressure and dimensionless pressure derivative for different values of L_D

t_D	L = 500 ft		L = 1,000 ft		L = 1,500 ft		L = 2,000 ft		L = 2,500 ft	
	P_D	P'_D	P_D	P'_D	P_D	P'_D	P_D	P'_D	P_D	P'_D
1.0×10^{-6}	0.0380	0.1214	0.2815	0.3537	0.4670	0.3483	0.4726	0.2858	0.5148	0.2452
1.0×10^{-5}	1.4428	1.0550	1.4990	0.6292	1.4027	0.4362	1.1987	0.3301	1.1114	0.2659
1.0×10^{-4}	4.2597	1.3097	3.0056	0.6665	2.4224	0.4461	1.9662	0.3349	1.7270	0.2681
1.0×10^{-3}	7.3198	1.3383	4.5463	0.6704	3.4511	0.4471	2.7380	0.3353	2.3446	0.2683
1.0×10^{-2}	10.406	1.3412	6.0905	0.6708	4.4807	0.4472	3.5102	0.3354	2.9623	0.2683
1.0×10^{-1}	13.494	1.3415	7.5076	0.9719	5.2914	0.7483	4.1033	0.6365	3.4605	0.5694
1.0×10^{0}	15.364	1.7175	8.3124	1.0468	6.0961	0.8232	4.9081	0.7114	4.2652	0.6443
1.0×10^{1}	16.244	1.7269	9.1928	1.0562	6.9765	0.8326	5.7885	0.7208	5.1456	0.6537
1.0×10^{2}	17.133	1.7279	10.166	1.8244	8.4036	1.9846	7.9464	4.9666	8.6829	6.8033
1.0×10^{3}	18.645	2.9414	15.934	10.284	21.823	19.675	32.336	32.677	46.753	49.024
1.0×10^{4}	33.658	22.567	77.104	76.732	158.62	164.35	276.24	287.07	427.45	442.85
1.0×10^{5}	186.66	183.87	689.10	705.33	1526.6	1557.2	2715.2	2759.3	4234.5	4291.3
1.0×10^{6}	1716.7	1740.1	6809.1	6877.8	15,207	15,316	27,105	27,254	42,304	42,493

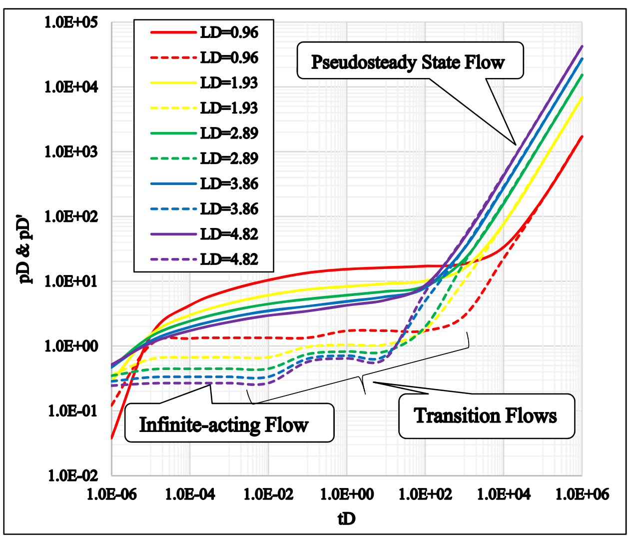

Figure 2: Variation in dimensionless pressure and dimensionless pressure derivative with L_D.

4.2 Effect of dimensionless reservoir length

To investigate the effect of dimensionless reservoir length, x_{eD} on the flow periods and dimensionless pressure, constant values of well and reservoir parameters are considered and the dimensionless reservoir length is varied. Table 4 shows the dimensional values considered and the computed dimensionless parameters.

Table 5 shows the dimensionless flow period times as computed using Odeh and Babu strategies. For the first two values of x_{eD} considered, it is observed that the x-boundary is felt earlier than the y-boundary and thus the dimensionless pressure is computed using equation (3) and the dimensionless pressure derivative is computed using equation (4). For the other values of x_{eD} considered, it is observed that the y-boundary is felt first and thus dimensionless pressure is computed using equation (1) and dimensionless pressure derivative is computed using

Table 4: Dimensional and dimensionless parameters for different values of x_{eD}

x (ft)	k_x = 200 md, k_y = 150 md, k_z = 10 md, L = 1,000 ft, h = 150 ft, y_e = 20,000 ft								
	L_D	x_{wD}	x_{eD}	r_{wD}	y_{wD}	y_{eD}	z_D	z_{wD}	h_D
5,000	1.9285	2.8927	5.7855	0.0016	13.3610	26.7219	0.3897	0.3881	0.7762
10,000	1.9285	5.7855	11.571	0.0016	13.3610	26.7219	0.3897	0.3881	0.7762
20,000	1.9285	11.571	23.142	0.0016	13.3610	26.7219	0.3897	0.3881	0.7762
40,000	1.9285	23.142	46.284	0.0016	13.3610	26.7219	0.3897	0.3881	0.7762
80,000	1.9285	46.284	92.568	0.0016	13.3610	26.7219	0.3897	0.3881	0.7762

Table 5: Dimensionless flow period times for different values of x_{eD}

x (ft)	Early radial		Early linear		Late pseudoradial			Late linear		
	t_{De}	t_{De}	$t_{D(start)}$	$t_{D(end)}$	$t_{D(start)}$	$t_{D(end)}$	$t_{D(end)}$	$t_{D(start)}$	$t_{D(start)}$	$t_{D(end)}$
5,000	0.0716	0.0442	0.0716	0.0566	0.5231	3.5788	77.761	6.7864	0.0716	77.761
10,000	0.0716	0.0442	0.0716	0.0566	0.5231	15.950	77.761	34.357	0.0716	77.761
20,000	0.0716	0.0442	0.0716	0.0566	0.5231	67.202	77.761	153.12	0.0716	77.761
40,000	0.0716	0.0442	0.0716	0.0566	0.5231	275.74	77.761	645.14	0.0716	77.761
80,000	0.0716	0.0442	0.0716	0.0566	0.5231	1117.0	77.761	2647.1	0.0716	77.761

Table 6: Dimensionless pressure and dimensionless pressure derivative for varying reservoir length, x_{eD}

t_D	x = 5,000 ft		x = 10,000 ft		x = 20,000 ft		x = 40,000 ft		x = 80,000 ft	
	P_D	P_D'	P_D	P_D'	P_D	P_D'	P_D	P_D'	P_D	P_D'
1.0×10^{-6}	0.2815	0.3537	0.2815	0.3537	0.2815	0.3537	0.2815	0.3537	0.2815	0.3537
1.0×10^{-5}	1.4990	0.6292	1.4990	0.6292	1.4990	0.6292	1.4990	0.6292	1.4990	0.6292
1.0×10^{-4}	3.0056	0.6665	3.0056	0.6665	3.0056	0.6665	3.0056	0.6665	3.0056	0.6665
1.0×10^{-3}	4.5463	0.6704	4.5463	0.6704	4.5463	0.6704	4.5463	0.6704	4.5463	0.6704
1.0×10^{-2}	6.0905	0.6708	6.0905	0.6708	6.0905	0.6708	6.0905	0.6708	6.0905	0.6708
1.0×10^{-1}	7.5076	0.9719	7.5076	0.9719	7.5076	0.9719	7.5076	0.9719	7.5076	0.9719
1.0×10^{0}	8.3124	1.0468	8.3124	1.0468	8.3124	1.0468	8.3124	1.0468	8.3124	1.0468
1.0×10^{1}	9.2714	1.7032	9.1928	1.0562	9.1928	1.0562	9.1928	1.0562	9.1928	1.0562
1.0×10^{2}	12.489	7.1632	10.725	4.1102	10.166	1.8244	10.166	1.8244	10.166	1.8244
1.0×10^{3}	49.029	48.127	28.995	24.592	19.084	13.584	14.339	8.5842	13.485	3.4842
1.0×10^{4}	414.43	427.52	211.69	214.29	109.98	109.73	60.239	59.732	34.910	33.732
1.0×10^{5}	4068.4	4125.8	2038.7	2063.4	1019.0	1035.3	519.24	535.33	259.91	275.33
1.0×10^{6}	40,608	40,805	20,309	20,403	10,109	10,178	5109.2	5177.8	2509.9	2577.8

equation (2). Table 6 shows the computed values of dimensionless pressure and dimensionless pressure derivative.

Figure 3 shows the plots of P_D and P_D' against t_D on log–log axes where the solid lines represent P_D against t_D, while the dashed lines represent P_D' against t_D.

From the parameters considered, for all the values of x_{eD}, an infinite-acting flow is identified from the time the well is put into production. This flow is radial in the y–z plane and considered as the early radial flow period. This is evident in the flattening of the graph of dimensionless pressure derivative during early time. It is noted that the early radial flow period will end when the wellbore end effects start affecting the flow. This is followed by a transition flow until the vertical boundary is felt. When the vertical boundary is felt, a transition flow is identified which prevails until the flow starts coming from beyond the ends of the wellbore. This is indicated in the plot by an upward straight line. When the flow starts coming from beyond the ends of the wellbore, a radial flow in the x–y plane is

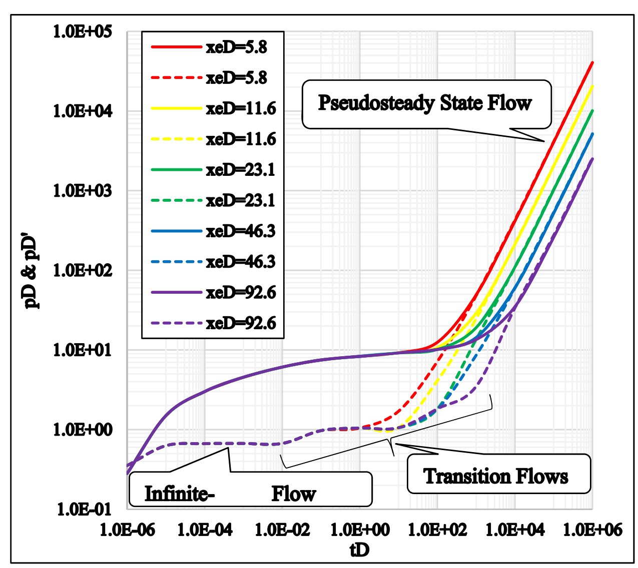

Figure 3: Variation in dimensionless pressure and dimensionless pressure derivative with x_{eD}.

Table 7: Dimensional and dimensionless parameters for different values of y_{eD}

y (ft)	k_x = 200 md, k_y = 150 md, k_z = 10 md, L = 1,000 ft, h = 150 ft, x_e = 20,000 ft								
	L_D	x_{wD}	x_{eD}	r_{wD}	y_{wD}	y_{eD}	z_D	z_{wD}	h_D
5,000	1.9285	11.571	23.142	0.0016	3.3402	6.6805	0.3897	0.3881	0.7762
10,000	1.9285	11.571	23.142	0.0016	6.6805	13.361	0.3897	0.3881	0.7762
20,000	1.9285	11.571	23.142	0.0016	13.361	26.722	0.3897	0.3881	0.7762
40,000	1.9285	11.571	23.142	0.0016	26.722	53.444	0.3897	0.3881	0.7762
80,000	1.9285	11.571	23.142	0.0016	53.444	106.89	0.3897	0.3881	0.7762

identified which is considered as the late pseudoradial flow period with the flattening of the plot. For the first three values of x_{eD} considered, it is noted that this flow ends when the x-boundary starts having effects on the flow and for the last two values of x_{eD} considered, it ends when the y-boundary is felt. For the first two cases of x_{eD} considered, a transition flow is identified which prevails until the x-boundary is felt. When the x-boundary is felt, a linear flow in the x–y plane is identified which prevails until the y-boundary is felt. This flow can be considered as the late linear flow period and evident with the straight upward line. For the third case of x_{eD} considered, a short transition flow is identified from the time the late pseudoradial flow ends until the time when y-boundary is felt. For the last three cases of x_{eD} considered, when the y-boundary is felt, a transition flow is identified that prevails until the x-boundary is felt. This transition flow is evident with the upward straight line in the dimensionless pressure derivative graph. When all the boundaries have been felt, a pseudosteady state behaviour is identified with an upward straight line in the dimensionless pressure derivative graph. This flow will prevail for the rest of the productive life of the well. It is observed that there is no effect on the change in dimensionless reservoir length on the pressure response during early time. However, this is not the case as observed during middle and late times. During these times, we note that as the dimensionless reservoir length increases, the pressure response decreases with a large decrease during late times.

4.3 Effect of dimensionless reservoir width

Since it is expected that the dimensionless reservoir width, y_{eD} will have an effect on the flow periods prevalence time, it is expected to have an effect on the pressure response.

To investigate this effect, constant well and reservoir parameters are considered and the dimensionless reservoir width is varied. Table 7 shows the dimensional values considered and the dimensionless parameters computed. Table 8 shows the dimensionless flow period times as computed using Odeh and Babu strategies. For the first three values of y_{eD} considered, it is observed that the y-boundary is felt first and thus dimensionless pressure is computed using equation (1) and dimensionless pressure derivative is computed using equation (2). For the last two values of y_{eD} considered, it is observed that the x-boundary is felt first and thus dimensionless pressure is computed using equation (3) and dimensionless pressure derivative is computed using equation (4). The computed values of dimensionless pressure and dimensionless pressure derivative are shown in Table 9.

Figure 4 shows the plots of P_D and P_D' against t_D on log–log axes where the solid lines represent P_D against t_D, while the dashed lines represent P_D' against t_D. From the parameters considered, an infinite-acting flow period is identified from the time the well is put into production. This flow period is radial in the y–z plane and considered to be the early radial flow period. This is evident as seen

Table 8: Dimensionless flow period times for different values of y_{eD}

y (ft)	**Early radial**		**Early linear**		**Late pseudoradial**			**Late linear**		
	t_{De}	t_{De}	$t_{D(start)}$	$t_{D(end)}$	$t_{D(start)}$	$t_{D(end)}$	$t_{D(end)}$	$t_{D(start)}$	$t_{D(start)}$	$t_{D(end)}$
5,000	0.0716	0.0442	0.0716	0.0566	0.5231	67.202	4.8601	153.12	0.0716	4.8601
10,000	0.0716	0.0442	0.0716	0.0566	0.5231	67.202	19.440	153.12	0.0716	19.440
20,000	0.0716	0.0442	0.0716	0.0566	0.5231	67.202	77.761	153.12	0.0716	77.761
40,000	0.0716	0.0442	0.0716	0.0566	0.5231	67.202	311.05	153.12	0.0716	311.05
80,000	0.0716	0.0442	0.0716	0.0566	0.5231	67.202	1244.2	153.12	0.0716	1244.2

Table 9: Dimensionless pressure and dimensionless pressure derivative for varying reservoir width, y_{eD}

t_D	y = 5,000 ft		y = 10,000 ft		y = 20,000 ft		y = 40,000 ft		y = 80,000 ft	
	P_D	P'_D	P_D	P'_D	P_D	P'_D	P_D	P'_D	P_D	P'_D
1.0×10^{-6}	0.2815	0.3537	0.2815	0.3537	0.2815	0.3537	0.2815	0.3537	0.2815	0.3537
1.0×10^{-5}	1.4990	0.6292	1.4990	0.6292	1.4990	0.6292	1.4990	0.6292	1.4990	0.6292
1.0×10^{-4}	3.0056	0.6665	3.0056	0.6665	3.0056	0.6665	3.0056	0.6665	3.0056	0.6665
1.0×10^{-3}	4.5463	0.6704	4.5463	0.6704	4.5463	0.6704	4.5463	0.6704	4.5463	0.6704
1.0×10^{-2}	6.0905	0.6708	6.0905	0.6708	6.0905	0.6708	6.0905	0.6708	6.0905	0.6708
1.0×10^{-1}	7.5076	0.9719	7.5076	0.9719	7.5076	0.9719	7.5076	0.9719	7.5076	0.9719
1.0×10^{0}	8.3124	1.0468	8.3124	1.0468	8.3124	1.0468	8.3124	1.0468	8.3124	1.0468
1.0×10^{1}	9.5007	2.0244	9.1928	1.0562	9.1928	1.0562	9.1928	1.0562	9.1928	1.0562
1.0×10^{2}	13.696	4.1265	11.165	2.5920	10.166	1.8244	10.082	1.0572	10.082	1.0572
1.0×10^{3}	49.536	51.366	29.085	26.212	19.084	13.584	14.299	7.7764	12.218	2.6764
1.0×10^{4}	414.94	437.76	211.79	219.41	109.98	109.73	60.200	57.177	34.481	31.177
1.0×10^{5}	4068.9	4158.1	2038.8	2079.6	1019.0	1035.3	519.20	527.25	259.48	267.25
1.0×10^{6}	40,609	40,908	20,309	20,455	10,109	10,178	5109.2	5152.3	2509.5	2552.3

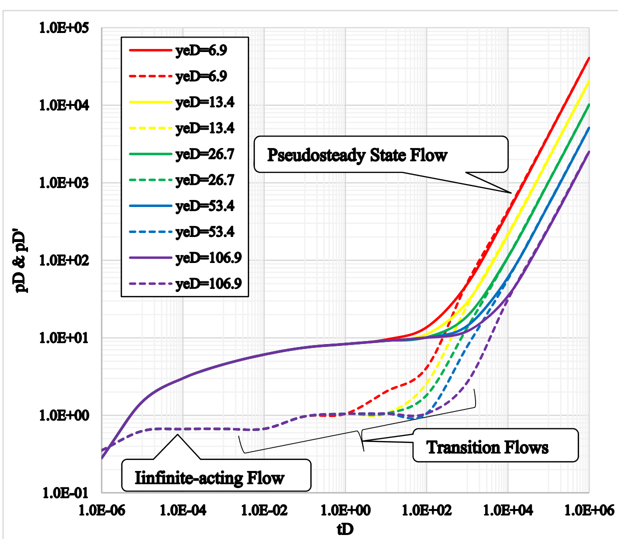

Figure 4: Variation in dimensionless pressure and dimensionless pressure derivative with y_{eD}.

from the flattening of the graph of dimensionless pressure derivative during early time. The identified early radial flow is observed to end when the wellbore end effects start affecting the flow. At this point a transition flow is identified which prevails until the vertical boundary is felt. When the vertical boundary is felt, a transition flow that prevails until the flow starts coming from beyond the ends of the wellbore is also identified. This is identified in the graph of dimensionless pressure derivative with an upward straight line. At the point when the flow starts coming from beyond the ends of the wellbore, a radial flow in the x–y plane considered to be the late pseudoradial flow period is identified. For the first two cases of y_{eD} considered, it is observed that this flow will end when the y-boundary is felt. For the last three values of y_{eD} considered, it is observed that this flow ends when the x-boundary starts having an effect on the flow. This flow is evident with the flattening of the dimensionless pressure derivative graph. Analysing the third value of y_{eD} considered, a short transition flow is identified after the late pseudoradial flow period ends. This transition flow ends when the y-boundary is felt. For the first three cases of y_{eD} considered, when the y-boundary is felt, a transition flow is identified and it prevails until the x-boundary is felt. This flow is identified from the straight upward line on the plot of dimensionless pressure derivative. For the last two cases of y_{eD} considered, when the x-boundary is felt, a linear flow in the x–y plane which can be considered as the late linear flow period is also identified.

This flow is evident in the plot of dimensionless pressure derivative by the upward straight line. This flow period will end when all the boundaries have been felt. At this point, a pseudosteady state behaviour is evident with a straight upward line. It is also noted that as much as the increase in dimensionless reservoir width has no effect on the pressure response during early time, it shows a decrease in pressure response during late time. Further, it is noted that an increase in the dimensionless reservoir width increases the prevalence time of the late pseudoradial flow period.

5 Conclusion

The study investigated how well design and reservoirs geometry affected the overall performance of a horizontal well in a completely bounded reservoir throughout its productive life. A horizontal well in a rectangular reservoir with completely sealed boundaries was considered and the effect of dimensionless well length L_D, dimensionless reservoir length x_{eD}, and dimensionless reservoir width, y_{eD} on pressure response over a given period of production using dimensionless time, t_D was studied. Appropriate well and reservoir parameters were considered and the respective dimensionless parameters were computed which were then used in computing dimensionless pressure P_D and its dimensionless pressure derivative P_D'. From the computations, the results obtained were analysed in diagnostic log–log plots with a discussion of the flow periods.

From this study, the dimensionless horizontal well length and the reservoir geometry have an effect on flow periods and influence how a horizontal well performs from inception to date. It is observed that

(1) From the time when the well is put into production, as many as seven flow periods can occur from the infinite-acting flow to full pseudosteady state behaviour. However, when considering the effect of boundaries separately, only five mathematical models are applicable.

(2) Longer horizontal wells will experience low pressure response during early time but this will increase at late times. The results obtained indicate that an increase in dimensionless well length decreases pressure response during the infinite-acting flow at early times and during transition flows at middle time but increases the pressure response during the pseudosteady state flow at late times.

(3) Large drainage volumes will have a reduced pressure response at late times. The dimensionless reservoir width and length are observed not to influence dimensionless pressure response during the infinite-acting flow at early times and during the transition flows at middle time, only affecting the prevalence time of the flow periods. However, it is observed that during the pseudosteady state flow at late times, dimensionless pressure response reduces with increased dimensionless reservoir length and width.

Nomenclature

h	reservoir thickness, ft
h_D	dimensionless reservoir thickness
k	reservoir permeability, md
k_x	directional permeability in the x-direction, md
k_y	directional Permeability in the y-direction, md
k_z	directional Permeability in the z-direction, md
L	well length, ft
P_D	dimensionless pressure
P_D'	dimensionless pressure derivative
s	source
t	time, h
t_D	dimensionless time
x	length in x-direction, ft
x_D	dimensionless reservoir length in the x-direction
x_e	reservoir length, ft
x_{eD}	external dimensionless reservoir length
x_w	source coordinate in the x-direction, ft
x_{wD}	dimensionless source coordinate in the x-direction
y	width in y-direction, ft
y_D	dimensionless reservoir width in the y-direction
y_e	reservoir width, ft
y_{eD}	external dimensionless reservoir width
y_w	source coordinate in the y-direction, ft
y_{wD}	dimensionless source coordinate in the y-direction
z	thickness in z-direction, ft
z_D	dimensionless reservoir thickness
z_w	source coordinate in the z-direction, ft
z_{wD}	dimensionless source coordinate in the z-direction
τ_D	dimensionless dummy variable for time

Conflict of interest: Authors state no conflict of interest.

References

[1] Adewole ES. The use of source and green's functions to derive dimensionless pressure and dimensionless pressure derivative distribution of a two-layered reservoir, part I: A-shaped architecture. J Math Technol. 2010;16:92–101.

[2] Al Rbeawi S, Tiab D. Transient pressure analysis of horizontal wells in a multi-boundary system. Am J Eng Res. 2013;2(4):44–66. doi: 10.2118/142316-MS.

[3] Carvalho RS, Rosa AJ. A mathematical model for pressure evaluation in an infinite-conductivity horizontal well. SPE Form Eval. 1989;4(4):559–66, SPE 15967. doi: 10.2118/15967-PA.

[4] Clonts MD, Ramey Jr HJ. Pressure transient analysis for wells with horizontal drain holes. Conference Paper Presented at the SPE California Regional meeting, Oakland, California; 1986, April 2–4. doi: 10.2118/15116-MS.

[5] Daviau F, Mouronval G, Bourdarot G, Curutchet P. Pressure analysis for horizontal wells. SPE Form Eval. 1988;3(4):716–24. doi: 10.2118/14251-PA.

[6] Eiroboyi I, Wilkie SI. Comparative evaluation of pressure distribution between horizontal and vertical wells in a reservoir (edge water drive). Niger J Technol. 2017;36(2):457–60. doi: 10.4314/njt.v36i2.19.

[7] Erhunmwun ID, Akpobi JA. Analysis of pressure variation of fluid in bounded circular reservoirs under the constant pressure outer boundary condition. Niger J Technol. 2017;36(1):461–8. doi: 10.4314/njt.v36i1.20.

[8] Goode PA, Thambynayagam RKM. Pressure drawdown and buildup analysis of horizontal wells in anisotropic media. Soc Pet Eng J. 1987;2(4):683–97. doi: 10.2118/14250-PA.

[9] Gringarten AC, Ramey HJ. The use of source and green's functions in solving unsteady - flow problems in reservoirs. Soc Pet Eng J. 1973;13(5):285–96. doi: 10.2118/3818-PA.

[10] Idudje EH, Adewole ES. A new test analysis procedure for pressure drawdown test of a horizontal well in an infinite-acting reservoir. Niger J Technol. 2020;39(3):816–20. doi: 10.4314/njt.v39i3.22.

[11] Kuchuk FJ, Goode PA, Wilkinson DJ, Thambynayagam RK. Pressure-transient behavior of horizontal wells with and without gas cap or aquifer. Soc Pet Eng. 1991;6(1):86–94. doi: 10.2118/17413-PA.

[12] Lee WJ. Well testing. New York: Society of Petroleum Engineers of AIME; 1982. p. 1–4.

[13] Mathews CS, Russell DG. Pressure buildup and flow tests in wells, monograph. Vol. I. Dallas, TX: Society of Petroleum Engineers of AIME; 1967.

[14] Odeh AS, Babu DK. Transient Flow Behaviour of Horizontal Wells, Pressure Drawdown, and Buildup Analysis. Conference Paper Presented at the SPE California Regional Meeting, Bakersfield, California; 1989, April 5–7. doi: 10.2118/18802-MS.

[15] Ogbamikhumi AV, Adewole ES. Pressure behaviour of a horizontal well sandwiched between two parallel sealing faults. Niger J Technol. 2020;39(1):148–53. doi: 10.4314/njt.v39i1.16.

[16] Oloro JO, Adewole ES, Olafuyi OA. Pressure distribution of horizontal wells in a layered reservoir with simultaneous gas cap and bottom water drive. Am J Eng Res. 2014;3(12):41–53.

[17] Oloro JO, Adewole ES. Derivation of pressure distribution models for horizontal well using source function. J Appl Sci Environ Manag. 2019;23(4):575–83. https://www.ajol.info/index.php/jasem.

[18] Orene JJ, Adewole ES. Pressure distribution of horizontal well in a bounded reservoir with constant pressure top and bottom. Niger J Technol. 2020;39(1):154–60. doi: 10.4314/njt.v39i1.17.

[19] Owolabi AF, Olafuyi OA, Adewole ES. Pressure distribution in a layered reservoir with gas-cap and bottom water. Niger J Technol. 2012;31(2):189–98.

[20] Ozkan, E, Raghavan, R, Joshi, S. Horizontal Well Pressure Analysis. Conference Paper Presented at the SPE California Regional Meeting, Ventura, California; 1987, April 8–10. doi: 10.2118/16378-PA.

[21] Nzomo T, Adewole S, Awuor K, Okang'a Oyoo D. Performance of a horizontal well in a bounded anisotropic reservoir: Part I: Mathematical analysis. Open Eng. 2022;12(1):17–28. doi: 10.1515/eng-2022-0003.

[22] Nzomo TK, Adewole SE, Awuor KO, Oyoo DO. Mathematical description of a bounded oil reservoir with a horizontal well: Early time flow period. Afr J Pure Appl Sci. 2021;2(1):67–76. doi: 10.33886/ajpas.v2i1.190.

[23] Nzomo TK, Adewole SE, Awuor KO, Oyoo DO. Mathematical description of a bounded oil reservoir with a horizontal well: Late time flow period. Afr J Pure Appl Sci. 2021;2(1):61–6. doi: 10.33886/ajpas.v2i1.188.